Weierstraß-Institut

für Angewandte Analysis und Stochastik

Leibniz-Institut im Forschungsverbund Berlin e. V.

Spatial rocking phenomenon in broad area semiconductor lasers

Mindaugas Radziunas[1], Kestutis Staliunas[2,3]

submitted: March 17, 2011

[1] Weierstrass Institute
     Mohrenstr. 39
     10117 Berlin, Germany
     E-Mail: Mindaugas.Radziunas@wias-berlin.de

[2] Departament de Física i Enginyeria Nuclear,
     Universitat Politècnica de Catalunya,
     Colom 11, 08222 Terrassa,
     Barcelona, Spain

[3] Institució Catalana de Reserca i Estudis Avançats (ICREA),
     Pg. Lluis Companys, 23, 08010,
     Barcelona, Spain
     E-Mail: kestutis.staliunas@icrea.es

Abstract

The spatial "rocking" is a dynamical effect converting a phase-invariant oscillatory system into a phase-bistable one, where the average phase of the system locks to one of two values differing by π. We demonstrate theoretically the spatial rocking in experimentally accessible and practically relevant systems – the broad area semiconductor lasers. By numerical integration of the laser model equations we show the phase bistability of the optical fields and explore the bistability area in parameter space. We also predict the spatial patterns, such as phase domain walls and phase solitons, which are characteristic for the phase-bistable spatially extended pattern forming systems.

1   Introduction

The phenomenon of "rocking" has been proposed as a general effect in physics of dynamical systems, which converts the phase-invariant oscillatory system into a phase-bistable one where the average phase of the system locks to one of two values differing by π [1, 2]. Many nonlinear systems in nature and in technics, such as chemical, mechanical, biological or laser oscillators, display self-sustained oscillations with a particular amplitude and with free (invariant) phase. If such system is subjected to a resonant, or nearly-resonant additive signal, then the phase invariance of oscillations can be broken, and the frequency and phase of the system can lock to that of the external signal. If, however, the complex amplitude of external injection becomes periodic *in time* e.g. follows the harmonic oscillation law $\cos(\Omega t)$, then a pair of stable states with similar amplitudes but opposite phases can be obtained. In this case, the phase of the field averaged over a small time scale $\tau \propto \Omega^{-1}$ is no more invariant as in autonomous systems, and no more monostable as in systems with a constant injection, but rather becomes attracted by one of two values differing by π. In simple terms the phase of the oscillations "avoids" the states with the phases of injection (say 0 and π) and consequently "prefers" the states with the phases orthogonal to that of the injection ($\pi/2$ and $3\pi/2$). The phenomenon called by "rocking" was first predicted for a time-periodic injection signal [1] and later for a random in time injection signal [2]. This resulted in a phase-bistability of a "small", system with a relatively small number of the space degrees of freedom, which in optical case corresponds to the resonator with a small Fresnel number. For the systems of a large number of space degrees of freedom, the "rocking" results in excitation of spatial patterns such as rolls, phase domain walls and phase solitons [3]. Such patterns are typical for the phase-bistable spatially extended systems [4, 5, 6, 7, 8].

More recently the *spatial* "rocking" was proposed, where the complex amplitude of injection is a π-alternating periodic function *in space* on a relatively small space scale [9]. The spatial rocking, similarly to the temporal rocking, results in a phase-bistable dynamics of a "small" system, and in phase-bistable patterns in a spatially extended system. The spatial rocking has been predicted

[9] for a general case of dynamical systems, on basis of the model of the periodically in space driven Complex Ginzburg-Landau Equation (CGLE). On one hand this shows the universality of the phenomenon of spatial rocking, as the CGLE is a universal equation – a normal form of the Hopf bifurcation in a homogeneous media. On the other hand this does not prove the effect in any concrete physical system, as no real system is governed *exactly* by the CGLE. In this way the spatial rocking has never been demonstrated for any concrete physical system up to now.

The CGLE is a good, however idealized model for a certain type of broad area lasers. Namely, this model assumes a single longitudinal mode operation and a class-A or class-C laser type, where the material variables relax faster or at least with the same rate as the optical field in the resonator. In the present paper we demonstrate numerically that the spatial rocking can be also obtained in a class-B broad area (BA) semiconductor laser, which is a widespread and practically relevant system. We show this by simulating the traveling-wave (TW) equation model for the BA lasers [10, 11, 12] using realistic parameters [12, 13]. To realize the rocking we consider a periodic in space injection formed by two, coherently interfering at some angle, beams (fig. 1). We demonstrate typical features of spatial rocking, such as the locking of the phase of emitted beam to one of two values differing by π. We explore the range of efficient rocking and show that the effect is robust and could be observed experimentally. We also demonstrate typical spatial patterns induced by rocking, which are the phase domains and the phase solitons.
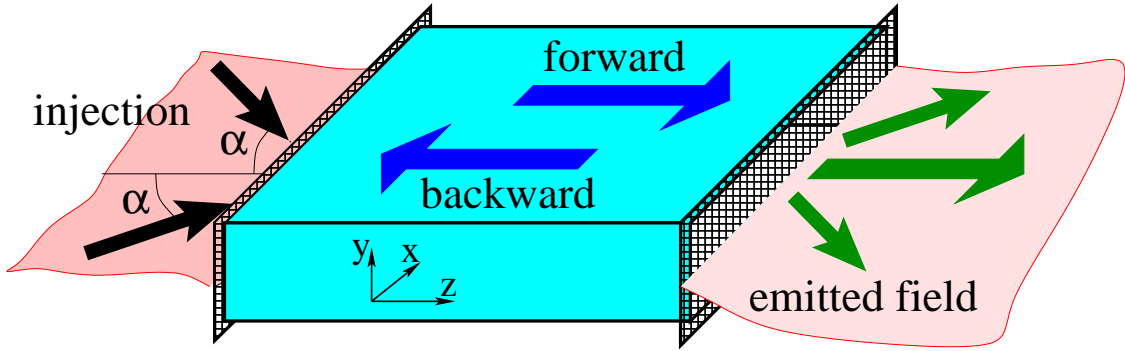
Figure 1: Schematic representation of the simulated system. The directions of injection and emission are shown by arrows.

2 Model

We consider the following TW model [10, 11, 12] for BA lasers:

$$\partial_t E^{\pm} = \frac{c}{n_g}\left(\frac{-i}{2k_0\bar{n}}\partial_{xx} \pm \partial_z - i\beta - \frac{c}{n_g}\frac{\bar{g}}{2}\right)E^{\pm} + \frac{\bar{g}}{2}p^{\pm},$$

$$\partial_t p^{\pm} = \frac{k_0 c}{2\lambda_0}\bar{\Gamma}\left(E^{\pm} - p^{\pm}\right) - \frac{ik_0 c}{\lambda_0}\bar{\lambda}_0 p^{\pm},$$

$$\partial_t N = d_N\partial_{xx}N + \frac{J(x,z)}{qd} - R(N) - \frac{c}{n_g}\Re e\sum_{\nu=\pm} E^{\nu*}\left(\left(g\left(N, E^{\pm}\right) - \bar{g}\right)E^{\nu} + \bar{g}p^{\pm}\right).$$

2

Here t denotes time, z – longitudinal coordinate, along the propagation direction, x – transverse coordinate. $E^{\pm}(t, x, z)$ are the complex slowly varying amplitudes of the forward and backward traveling optical fields, so that $|E|^2 = |E^+|^2 + |E^-|^2$ denotes the local photon density. $p^{\pm}(t, x, z)$ are the complex slowly varying amplitudes of induced polarization used to model the Lorentzian wavelength dependence of the optical gain. $N(t, x, z)$ is the real-valued distribution of excess carrier density. The injection current density J is given by

$$J(x, z) = \begin{cases} I/wl, & \text{if} \quad (x, z) \in S = \left\{ \left(-\frac{w}{2}, \frac{w}{2} \right) \times (0, l) \right\} \\ 0, & \text{elswhere} \end{cases},$$

were S and I denote the laser area and the injection current, respectively. The complex propagation factor β, the peak gain function g, the refractive index change function δ_n, and the carrier recombination function R are given by

$$\beta = \delta_n(N) + i\frac{g(N, E^{\pm}) - \gamma}{2}, \quad g(N, E^{\pm}) = \frac{g' \ln(N/N_{tr})}{1 + \epsilon|E|^2},$$

$$\delta_n(N) = -k_0\sqrt{n'N}, \quad R(N) = AN + BN^2 + CN^3.$$

At the laser facets the optical fields $E^{\pm}(t, x, z)$ satisfy the following boundary conditions:

$$E^+(t, x, 0) = r_0 E^-(t, x, 0) + a(t, x),$$

$$E^-(t, x, l) = r_l E^+(t, x, l).$$

Here $a(t, x)$ denotes the optical field injected into the laser through the left facet. We assume the injection in form of interference of two plane waves of opposite angles α and $-\alpha$ with respect to the optical axis of the laser, which results in harmonic function of the injection:

$$a(t, x) = a_0 e^{i\omega t} \sin(\alpha k_0 x).$$

Parameter ω is the optical frequency, relative to the reference frequency $\omega_0 = 2\pi c/\lambda_0$, while a_0 is the optical field amplitude determining power of optical injection:

$$P_{inj} = |a_0|^2 \int_{-w/2}^{w/2} \sin^2(\alpha k_0 x)\, dx \times \frac{cd}{n_g} \frac{hc}{\lambda_0}.$$

$k_0 = 2\pi/\lambda_0$, c, q and h denote the central wavenumber, the speed of light in vacuum, the electron charge, and the Planck constant, respectively. The values and the brief explanation of laser parameters are given in table 1. They correspond to the experimentally available BA semiconductor lasers and are discussed in more details in Refs. [12], [13]. Injected field power P_{inj} and the frequency detuning ω are the variable parameters of our system.

To resolve long transients and to perform a parameter continuation of the system in reasonable time we have used high performance parallel distributed computing algorithms [12]. Comparable computations on a single PC system take nearly 100 times longer.

Table 1: Parameters used in simulations.

$\bar{n}$	reference refractive index	3.2262
n_g	group refractive index	3.66
λ_0	central wavelength	973 nm
$\bar{g}$	Lorentzian gain amplitude	130 cm^{-1}
$\bar{\Gamma}$	Lorentzian width at half max.	80 nm
$\bar{\lambda}_0$	gain peak detuning	0 nm
I	injection current	3 A
g'	differential gain	23.4 cm^{-1}
γ	internal absorption	1.5 cm^{-1}
r_0	left facet ampl. reflectivity	-0.3
r_l	right facet ampl. reflectivity	0.3
N_{tr}	transparency carrier density	1.3$\cdot$10^{18} cm^{-3}
ϵ	nonlinear gain compression	5$\cdot$10^{-18} cm^3
n'	differential index	1.25$\cdot$10^{-25} cm^3
d_N	carrier diffusion coefficient	19.672 cm^2/s
l	length of the laser	1.5 mm
w	width of the laser	0.2 mm
d	thickness of active region	16 nm
A	recombination parameter	0.295$\cdot$10^9 s^{-1}
B	recombination parameter	1.8$\cdot$10^{-10} cm^3/s
C	recombination parameter	3.28$\cdot$10^{-30} cm^6/s
α	angle of the optical injection	0.05 rad.

3 Phase bistability

First we give a numerical proof of the efficient rocking. For considered injection current I the laser is pumped well above the threshold and, in the absence of optical injection, results in 1W field emission power. The multi-mode emission is observed, resulting in a random beat of many longitudinal and transverse modes. In this way the frequency spectrum and the far field (spatial spectrum) are irregular and broadened. This is a well known behavior of nonstabilized BA semiconductor lasers. In the presence of the optical injection $a(t,x)$ with properly selected frequency detuning and power ($\omega = 0$ and $P_{inj} = 0.2$W in this particular case) a typical to the rocked system behavior [9] is observed. Namely, depending on initial conditions, the state of the system is attracted by one of two stable attractors characterized by similar emitted field intensity but different field phases. The field intensity distributions shown in fig. 2 have a characteristic parallel-striped structure, with the stripe separation $\lambda_0/2\alpha$ and a typical alternation between more and less intensive stripes.

A confirmation of the efficient rocking is given in fig. 3, where thin black lines and dots show the computed near fields for both bistable states. Whereas the field intensities of both stable states (panels a and c) are similar, their phases (panels b and d) oscillate in space around one of two values differing by π. The computed fields are strongly modulated on a small spatial scale,

4
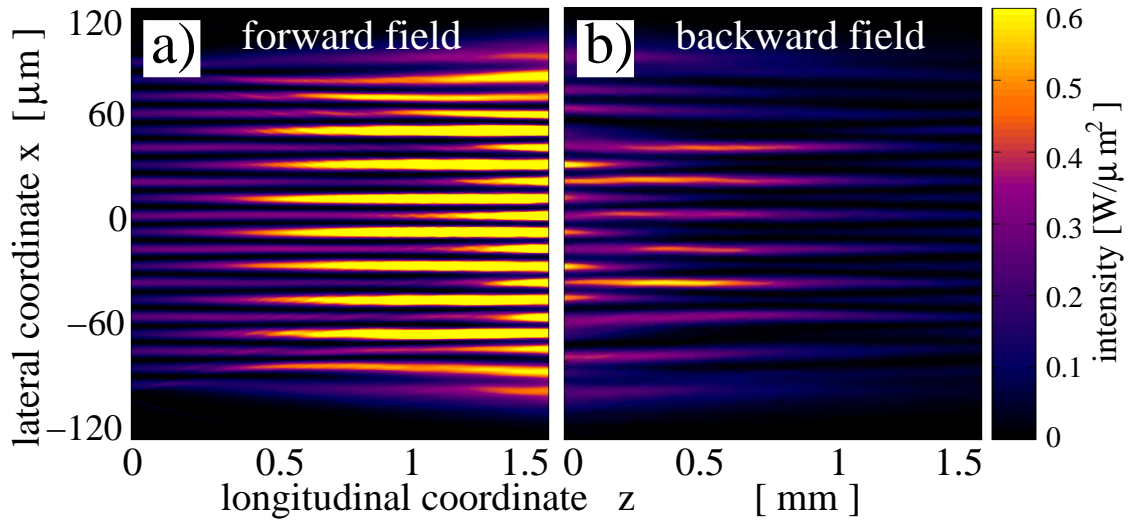
Figure 2: The characteristic 2D intensity distributions of the forward (a) and backward (b) waves, corresponding to one of bistable states. $\omega = 0$, $P_{inj} = 0.2$W. Other parameters as in table 1.
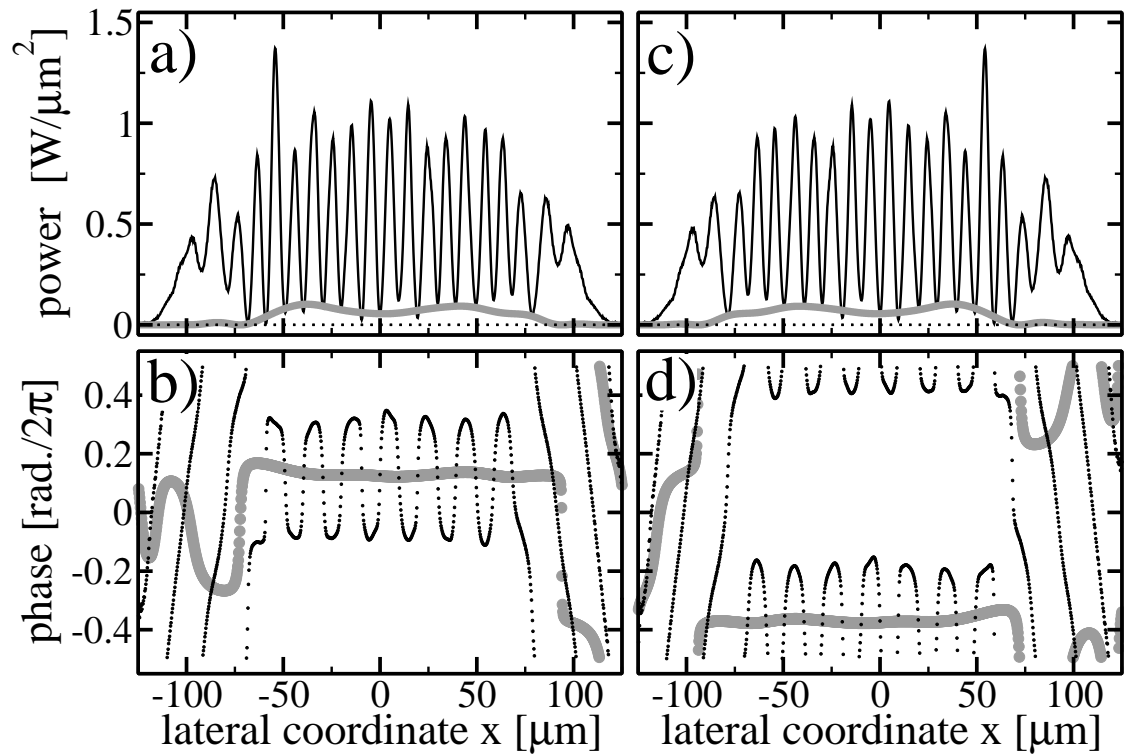
Figure 3: The intensity (a,c) and the phase (b,d) profiles of the fields emitted by laser for both (a,b) and (c,d) bistable states. The thin black and thick grey lines or dots represent the full- and small-scale-averaged distributions, respectively. All parameters as in fig. 2.

corresponding to the period of injection. This is what we call small scale modulation. As these field oscillations can cause confusion, we have also plotted the amplitudes and the phases of the fields averaged over the small space scale:[1] see thick grey lines and dots in fig. 3. After this averaging we get the relatively homogeneous distributions displaying no spatial patterns on the large space scale. The averaged field intensities approximately follow the lower border of the envelope of the computed oscillating field intensities. At the same time, the averaged field phases of both stable states are nearly constant within the central part of the simulated laser device and differ by π (grey dots in panels b and d).

4   Rocking area

To determine a parameter domain where the spatial rocking is efficient, we have performed a series of simulations varying the injected field power P_{inj} and the detuning ω.

We have started our simulations from the state reported in figs. 2 and 3(a,b). Then we have integrated the model equations for the time interval $t \in [0, N \cdot T]$ (N: number of small steps of parameter P_{inj}) estimating the simulated lasing state and slightly increasing (decreasing) parameter P_{inj} after each T-transient. This procedure allows to stay close to the same attractor in the phase space, to follow the deformations of this attractor in the parameter space, to detect its bifurcations and eventual transitions to another attractor. The results of this one-parameter continuation are summarized in Figs. 4a-c.

By performing similar 1-parameter continuations for several fixed frequency detuning ω we determine a border of the rocking area in two parameter plane. Fig. 4(d) presents this area in parameter space of the injected field frequency detuning and power (ω, P_{inj}).

The spatially rocked state is a continuous wave state possessing a single sharp line in the optical spectra (fig. 4a) and a non-vanishing zero-angle contribution in its far field (fig. 4b). The emitted field intensity shows no significant temporal oscillations (fig. 4c). The left (low injection) border of the rocking area is characterized by occurrence of temporal oscillations of the emitted field intensity and multiple modes in optical spectrum. The right (large injection) border can be recognized by a full suppression of the central peak in the far field.

Panels (a-c) of fig. 5 show different characteristics of typical rocked (b) and non-rocked (a,c) states. The analysis of all these states show:

  i) moderate power of the injection, where the rocking is obtained (panel b). Typical for the spatial rocking is the emission consisting of three well distinguishable far field peaks. While the side-peaks correspond mainly to the injected optical field, the central peak represents the space averaged lasing components, the phase of which is locked to one of two values differing by π. In this way, for the efficient rocking the existence of the central far-field peak is relevant. The optical frequency of the emitted field is determined by the optical injection frequency ω.

---

[1]We performed the averaging by i) transforming the fields into space Fourier domain, ii) filtering out the high spatial frequency components implied by the optical injection and retaining only the radiation around the central peak, and iii) transforming fields back to the space domain.
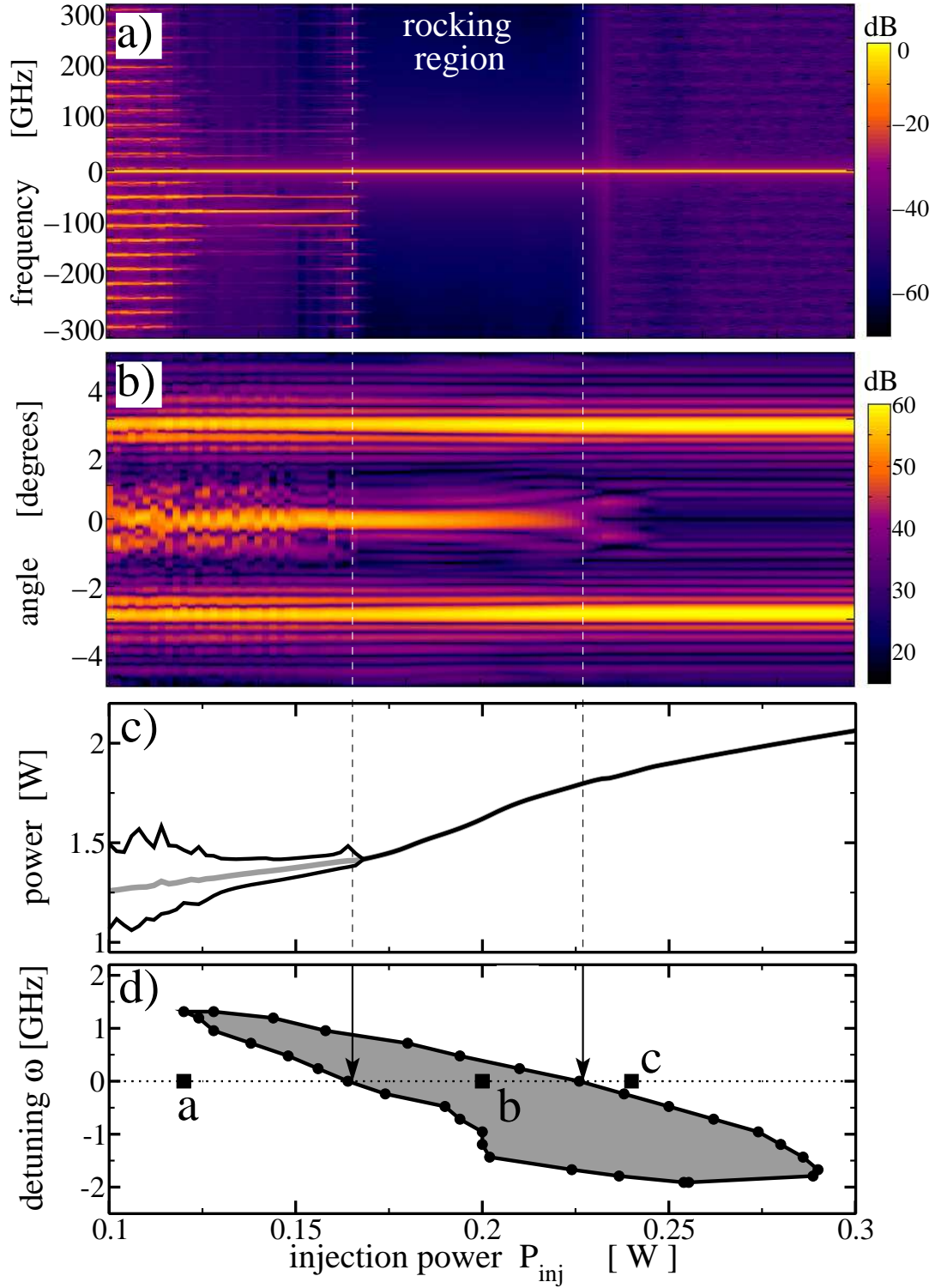
Figure 4: Stability area of the spatial rocking. Mappings of optical spectra (a), far fields (b), maximal, minimal and mean value of emitted power (c) for tuned injection power P_{inj} and fixed frequency detuning $\omega = 0$. Vertical dashed lines denote borders of stability of the rocking state. (d) The area in the parameter space of ω and P_{inj} resulting in a stable rocking (the "rocking" area). Parameters as in table 1.
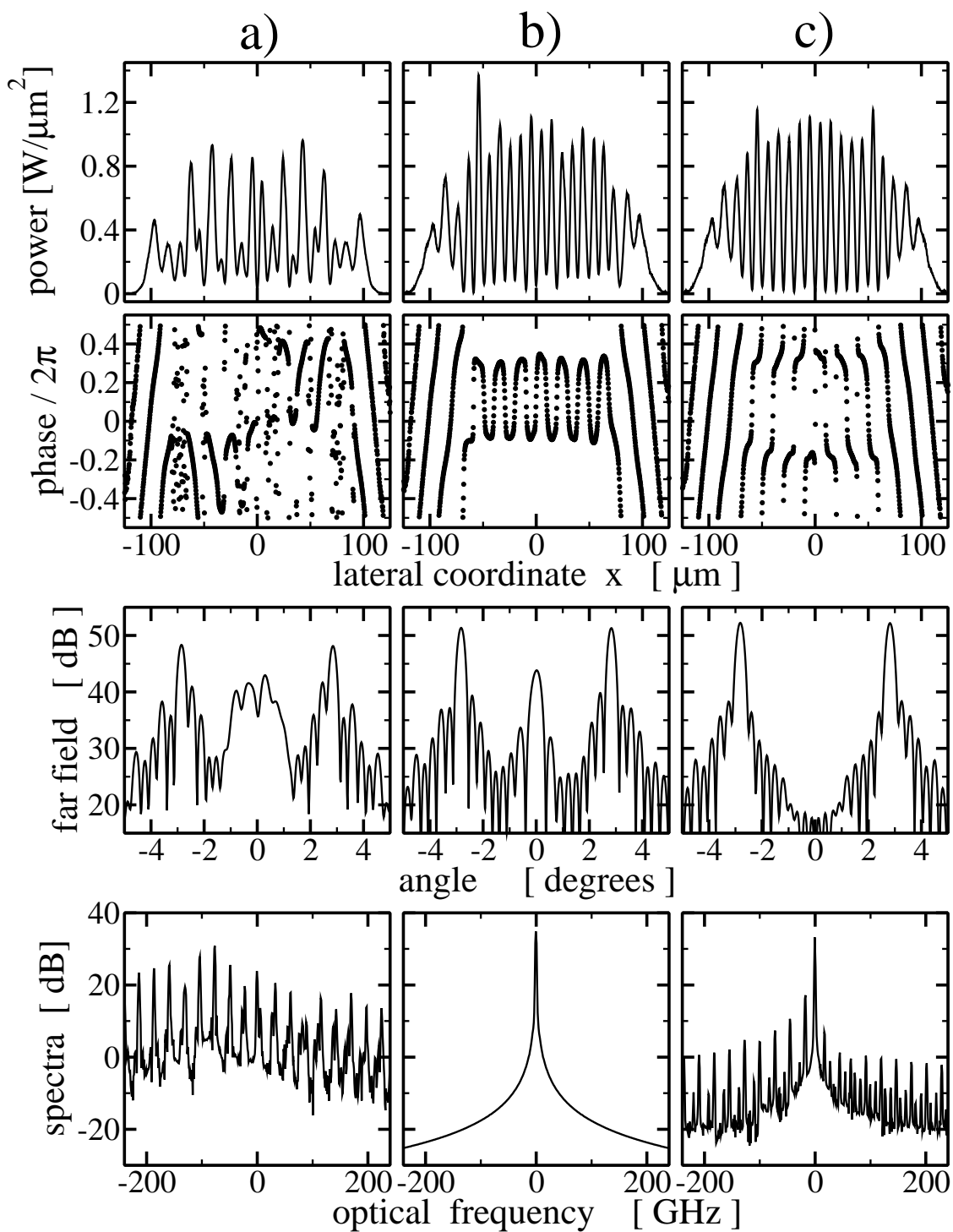
Figure 5: Typical "rocked" and "nonrocked" field configurations. Up to down: time averaged near field intensities and phases, time averaged far fields and optical spectra. The parameters P_{inj} and ω correspond to the positions of thick squares in fig. 4(d). Other parameters as in table 1.

ii) too large power of the injection (panel a). In this case the central (lasing) component of the far field is suppressed, and the laser is completely enslaved by the injection. The laser does not emit by itself, but acts as an amplifier of the injected field. The behavior, in principle, corresponds to that of injection locked laser, while the far field and the optical spectrum of laser follows that of the injection.

iii) too small power of the injection (panel c). In this case the injection is too weak to achieve a locking of the laser field phase to one of two bistable values. The spatial-temporal dynamics of the system resembles the random and noisy dynamics of the free-running broad emission area laser. However, not very far from the border of the rocking domain, one can recognize the concentration of the temporally evolving field phases at one of two values, which is a precursor of the phase bistability.

Typically the boundary of the rocking area from the left side shows a resonance-like shape, resembling the well known Arnold tongue in parametrically driven system. In the simplest cases the rocking area from the left follows $a_0 \propto |\omega|$ [9], however here the situation is more involved. Most importantly the rocking area is asymmetric with respect to the frequency detuning. The increasing optical injection power implies a decrease of the mean carrier density. This in turn causes a nonlinear refractive index shift, i.e., the nonlinear red-wavelength shift of the resonance frequency. As the consequence the rocking area is "tilted" in the plane of (ω, P_{inj}).

The latter diagram indicates that the rocking can be experimentally realized as the bistability area is sufficiently large in parameter space. The injection amplitude can be varied substantially, i.e. can be increased to the values comparable with the amplitude of the free running laser. The detuning can be varied over a substantial part of the free spectral range (around 12% for this concrete sample).

5 Patterns

Next we report the spatial patterns emerging on a large space scale. These patterns are typical for the systems with phase bistability, in particular, in parametrically driven systems [7]. The geometry of the laser simulated by us is such that the system is neither of "large", nor of "small" aspect ratio, as the Fresnel number of the resonator $F = \bar{n} w^2 / (\lambda_0 l) \approx 88$. In this way the system displays the phase-bistable homogeneous states (reported above), but also contains sufficient amount of spatial degrees of freedom for most simple transverse patterns.

The most simple pattern of the phase bistable system is the phase domain boundary: if in two neighboring lateral regions both stable solutions with opposite values of the averaged phase are realized, then in between a domain boundary must appear separating these two phase domains. The domain boundary obtained by numerical integration is shown in figs. 6a and b. The amplitude and the phase distributions of the averaged fields clearly indicate the presence of the domain wall with $\tanh (x/x_0)$ shape, which is typical for the Ising domain boundaries [7]. It is a heteroclinic connection between two phase bistable states, where the complex field goes through zero of the complex plane: see the intensity of the small-scale-averaged field dropping down to zero at $x \approx 0$ in fig. 6a.
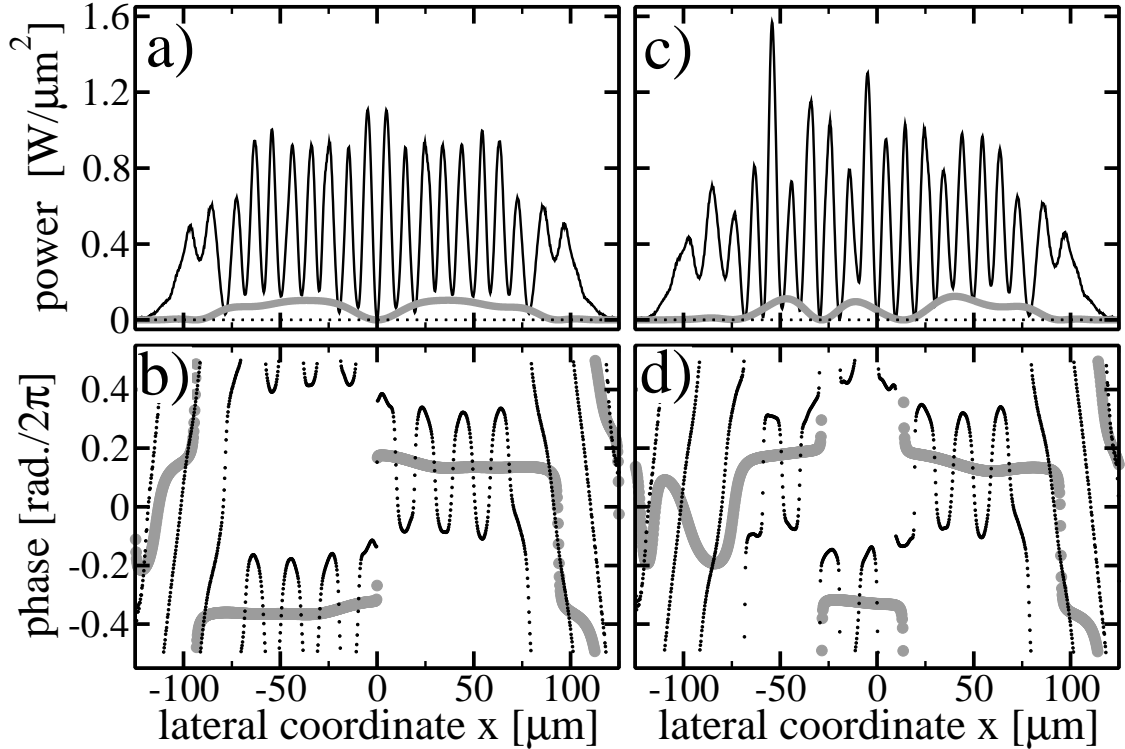
Figure 6: The spatial patterns: (a, b)-the Ising phase domain boundaries; (c, d)-phase solitons. The meaning of all dots and lines as in fig. 3. All parameters as in fig. 2.

When two Ising domain boundaries of the opposite polarities $\tanh\left(x/x_0\right)$ and $\tanh\left(-x/x_0\right)$ are located sufficiently close one to another, they may mutually lock, resulting in spatial phase soliton [14]. Such phase soliton is a homoclinic connection where the order parameter starts and ends on one bistable state and "visits" the other phase state passing two times the zero of complex plane. Such stable solitons were obtained in our system, and are presented in figs. 6c and d. We note, that we have located these solitons only in a limited part of the rocking domain. This is in agreement with Ref. [14], where the conditions ensuring a relatively strong mutual locking of the phase fronts of different polarity were calculated. The detailed analysis of the phase solitons in spatially rocked system, however, is behind the scope of the present letter.

6 Conclusions

Summarizing, we show numerically that the spatial rocking is realizable in realistic physical system – the broad area semiconductor laser. The substantial size of calculated phase-bistability area in parameter space let us believe that the spatial rocking in BA lasers can be observed experimentally. The homogeneous (on a large space scale) bistable solutions were found in the whole rocking area, and the patterns, characteristic to phase-bistable extended systems, were obtained in a part of the area.

We demonstrated the phase domains and phase-solitons. For the realization of more compli-

10

cated patterns of phase-bistable systems, like rolls, or soliton ensembles [6] the size of the simulated system was too small.

We note, that the effect of spatial rocking is substantially stronger for semiconductor laser, than the temporal rocking. The temporal rocking is known to be quite inefficient in stiff systems, such as class-B lasers, where the rocking area shrinks critically around the frequency of relaxation oscillations [15]. The semiconductor lasers belong to the class-B, where the material relaxation time is by three orders of magnitude larger than the photon live time in resonator. However we find that the spatial rocking is indeed very efficient here. Generally the spatial rocking seems to be not influenced by stiffness. Whereas in temporal rocking case one always deals with fast oscillation in time, in the spatial rocked states the temporal dynamics is eliminated, and the relaxation rates do not play a role in the process any more.

The spatial rocking in this particular system can have a practical relevance. The large active region of BA laser enables the high power of output field, which, however, usually is composed from multiple lateral modes, therefore the beam is of poor spatial and temporal quality [16]. Stabilization of some lateral mode in a BA laser can be achieved, for example, by a striped electrical contact design, by injection of the optical beam at some angle to the longitudinal axis [17] or by the external optical feedback from the corresponding off-axis mirror or grating [13]. The spatial rocking, apart from the phase bistability and the spatial patterns, allows also to improve the selectivity of the lateral modes and, therefore, the quality of the emitted beam.

Acknowledgments

References

[1] de Valcárcel G. J. and Staliunas K., *Phys. Rev. E* **67** (2003) p. 026604.

[2] Staliunas K. et al., *Phys. Rev. Lett.* **102** (2009) p. 010601.

[3] Esteban-Martin A. et al., *Phys. Rev. Lett.* **97** (2006) p. 093903.

[4] Cross M. C. and Hohenberg P. C., *Rev. Mod. Phys.* **65** (1993) p. 851.

[5] Walgraef D., Spatio-Temporal Pattern Formation, Springer, New York (1997).

[6] Staliunas K. and Sánchez-Morcillo V. J., Transverse Patterns in Nonlinear Optical Resonators, Springer, Berlin (2003).

[7] Coullet P. et al., *Phys. Rev. Lett.* **65** (1990) p. 1352.

[8] Coullet P. and Emilsson K., *Physica D* **61** (1992) p. 119.

[9] de Valcárcel G. J. and Staliunas K., *Phys. Rev. Lett.* **105** (2010) p. 054101.

[10] Balsamo S., Sartori F. and Montrosset I., *IEEE J. Sel. Topics Quantum Electron.* **2** (1996) p. 378.

[11] Egan A. et al., *IEEE J. Quantum Electron.* **34** (1998) p. 166.

[12] Spreemann M. et al., *IEEE J. Quantum Electron.* **45** (2009) p. 609.

[13] Jechow A. et al., *Optics Express* **17** (2009) p. 19599.

[14] Staliunas K. and Sánchez-Morcillo V. J., *Physics Letters A* **241** (1998) p. 28.

[15] Staliunas K. et al., *Opt. Commun.* **268** (2006) p. 160.

[16] Blaaberg S., Petersen P. M. and Tromborg B., *IEEE J. Quantum. Electron.* **43** (2007) p. 959.

[17] Hadley G. R., Owyoung A. and Hohimer J. P., *Optics Letters* **11** (1986) p. 144.